



Mixed matrix membranes containing MOFs for ethylene/ethane separation—Part B: Effect of Cu_3BTC_2 on membrane transport properties

Jeroen Ploegmakers, Susilo Japip, Kitty Nijmeijer*

Membrane Science & Technology, Mesa+ Institute for Nanotechnology, University of Twente, PO Box 217, Enschede 7500 AE, The Netherlands

ARTICLE INFO

Article history:

Received 21 September 2012

Received in revised form

30 October 2012

Accepted 2 November 2012

Available online 16 November 2012

Keywords:

Cu_3BTC_2

Gas separation

Ethylene

Mixed matrix membranes

Solubility

Diffusion

ABSTRACT

Mixed matrix membranes (MMMs) containing various amounts of the metal-organic framework (MOF) Cu_3BTC_2 as filler in P84 were characterized in terms of their ethylene and ethane separating performance. Previous research showed that especially the use of the MOF Cu_3BTC_2 improves the ethylene/ethane separating ability due its selective interaction with the olefin. Although the ethylene permeability remained constant, the ethylene/ethane permeability selectivity significantly increased to a value of 7.1 with increasing Cu_3BTC_2 loading. Experiments show that the ethylene solubility coefficient increased from 1.0 to $2.9 \times 10^{-3} \text{ mol}/(\text{m}^3 \text{ Pa})$ with increasing Cu_3BTC_2 loading up to 20 wt%. Since the ethylene permeability coefficient remained constant at $17 \times 10^{-18} \text{ mol m}/(\text{m}^2 \text{ s Pa})$ with increasing Cu_3BTC_2 loading, the ethylene diffusion coefficient was calculated to decrease by a factor of three. Evaluation of the reason for the strong increase in permeability selectivity with increasing Cu_3BTC_2 loading revealed that this is the result of an increase in diffusion selectivity by a factor of two. These results suggest immobilization of ethylene inside the MOF particles as the result of strong ethylene–copper(II) MOF interactions.

© 2012 Elsevier B.V. All rights reserved.

1. Introduction

Ethylene is one of the most important components in the petrochemical industry and used as resource for many products [1]. Due to their rather similar boiling points, both ethane and ethylene accumulate in the same naphtha fraction and highly selective separation processes are required to obtain high purity ethylene. Currently, distillation is used, which is an energy intensive process. Although membrane technology is a potential alternative, due to the Robeson permeability–selectivity tradeoff, polymer membrane performance is not sufficient yet and has to be improved to be an economically interesting alternative [2–4]. Addition of metal-organic framework (MOF) particles as additive to polymer membranes has already shown that permeability and selectivity can be simultaneously increased [5–11], but very little is known about the effect of these particles on the mechanism of gas transport and separation inside mixed matrix membranes (MMMs). Adams et al. studied the effect of CuTPA particles in PVA MMMs on not only the permeability and selectivity of various gasses, but also on the diffusion coefficient [12]. It was found that the diffusion coefficient decreased when particles were added as a result of penetrant immobilization. Unfortunately, only single gasses were tested and only low feed pressures ($< 5 \text{ bar}$) were considered.

This paper will thoroughly study the effect of the use of the MOF Cu_3BTC_2 [13] as additive in polymeric MMMs based on P84 on the ethylene and ethane transport properties. The structural formula of P84 can be found elsewhere [14]. Cu_3BTC_2 was chosen as previous research [15] showed that especially the use of this Cu(II) MOF showed selective interaction with the olefin and as such enhanced the separating ability of the membranes. Here we extend this study and elucidate the mechanism of the improved performance in terms of solubility, diffusion and permeability coefficients. We investigate the effect of the MOF loading on these properties. In addition, the effect of the feed pressures on the performance is investigated, to reveal the effect of the addition of MOFs on the high pressure stability of the polymer membranes.

2. Theory

2.1. Sorption

In order to examine the transport properties in MMMs, two aspects have to be considered. First, static sorption experiments can reveal the maximum sorption capacity of a certain gas in a polymer, which helps to understand why MOFs can enhance the performance of MMMs compared to native polymer membranes. Second, dynamic sorption experiments reveal information on the kinetics of the sorption behavior from which diffusion coefficients can be determined.

* Corresponding author. Tel.: +31 53 489 4185; fax: +31 53 4894611.
E-mail address: d.c.nijmeijer@utwente.nl (K. Nijmeijer).

2.2. Static sorption

Gas sorption in glassy polymeric membranes can be described by the dual mode sorption model [16], which assumes two different sorption mechanisms to take place simultaneously: Sorption directly proportional to the pressure following Henry's law, and Langmuir sorption, which relies on a hole-filling mechanism. In that case, the gas concentration inside the membrane, C (kmol/g), can be described by Eq. (1):

$$C = k_D \times p + \frac{C_H \times b \times p}{1 + b \times p} \quad (1)$$

where k_D is Henry's constant (kmol/(g bar)), p the pressure (bar), C_H the Langmuir capacity constant (kmol/g) and b the Langmuir affinity constant (1/bar). When gas mixtures are used or when the single gas parameters of two gasses are known, the two component dual-mode sorption can be applied if competitive sorption takes place and both gasses show dual mode sorption behavior. The concentration of component i (C_i (kmol/g)) inside the membrane is described by:

$$C_i = k_{Di} \times p_i + \frac{C_{Hi} \times b_i \times p_i}{1 + (b_i \times p_i) + (b_j \times p_j)} \quad (2)$$

where k_{Di} is Henry's constant (kmol/(g bar)), p_i the partial pressure (bar), C_{Hi} the Langmuir capacity constant (kmol/g) and b_i the Langmuir affinity constant (1/bar) for component i and b_j and p_j the Langmuir affinity constant (1/bar) and the partial pressure (bar) of component j , respectively. When multiple molecules adsorb on a single site, which often happens in case of metals, the Sips sorption model can be applied, which is a combination of Langmuir and Freundlich sorption, and is described by [17]:

$$C = \frac{C_S \times (b_S \times p)^{1/n}}{1 + (b_S \times p)^{1/n}} \quad (3)$$

where C_S (kmol/g) is the Sips capacity constant (kmol/g), b_S the Sips affinity constant (1/bar), p the pressure (bar) and n (–) the sorption intensity. Although Eq. (3) can be extended, analogous to Eq. (2), into a two component system, it must be stressed that even though single component Sips parameters can be accurately obtained from Eq. (3), multi-component sorption behavior cannot necessarily be predicted [18]. For this reason, Eq. (2) will be used throughout this report to predict multi-component sorption data in MMMs, while Eq. (3) will be used to create single component isotherms in MOFs. More information on the sorption models can be found elsewhere [19].

Once the concentration of a gas at a specific pressure is known, the solubility coefficient S ($\text{cm}^3/(\text{cm}^3 \text{cmHg})$) is defined by:

$$S = \frac{C}{p} \quad (4)$$

2.3. Dynamic sorption

Diffusion coefficients can be determined from dynamic sorption experiments. The analytical solution for gas diffusion D (cm^2/s), in uniform spherical particles, was given by Crank [20]:

$$\frac{m_t}{m_\infty} = 1 - \frac{6}{\pi^2} \sum_{n=1}^{\infty} \frac{1}{n^2} \exp\left[-\frac{4Dn^2\pi^2 t}{d^2}\right] \quad (5)$$

where m_t is the mass uptake (g) of a gas at time t (s), m_∞ mass uptake (g) at infinite time and d the particle diameter (cm). The diffusion coefficient can be accurately obtained given that the diffusion is constant and obeys Fick's laws throughout the entire experiment. Similar to Eq. (5), Crank showed that the Fickian

mass uptake, in a polymer film, can be written by Eq. (6):

$$\frac{m_t}{m_\infty} = 1 - \frac{8}{\pi^2} \sum_{n=0}^{\infty} \frac{1}{(2n+1)^2} \exp\left[-\frac{D(2n+1)^2\pi^2 t}{l^2}\right] \quad (6)$$

where l is the film thickness (cm) [21]. For both Eqs. (5) and (6) it is assumed that the gas concentration at the start of the experiment is 0 and that it is instantaneously increased after which there is a homogenous vapor phase concentration in equilibrium with the surface of the material. Berends and Hopfenberg showed that the model could also account for non-Fickian relaxation controlled swelling which often occurs in glassy polymers [22]:

$$\frac{m_t}{m_\infty} = m_{F,\infty} \left\{ 1 - \frac{8}{\pi^2} \sum_{n=0}^{\infty} \frac{1}{(2n+1)^2} \exp\left[-\frac{D(2n+1)^2\pi^2 t}{l^2}\right] \right\} + \sum_{i=1}^{\infty} m_{r,i} \left[1 - \exp\left(-\frac{t}{\tau_{r,i}}\right) \right] \quad (7)$$

where $m_{F,\infty}$ is the contribution of Fickian mass uptake at infinite time, $m_{r,i}$ the contribution of mass uptake due to additional relaxation i and $\tau_{r,i}$ is the characteristic time for relaxation i (s). Usually it is sufficient for glassy polymers to describe m_t/m_∞ by the addition of two relaxation regimes. It is assumed that the mass uptake of the relaxation regimes is independent of the Fickian sorption and both take place at different time scales. If the difference in timescale between the Fickian diffusion and the first, fast relaxational regime is too short, it is impossible to separate the two processes. To overcome this problem, membranes with a sufficiently low film thickness have to be selected to allow the Fickian mass uptake to be completed quickly. On the other hand, if the film thickness is too low, the Fickian mass uptake happens so quickly that it cannot be accurately measured as a result of instabilities in the electronic signal of the magnetic suspension balance caused by temperature fluctuations [23]. Given these difficulties, an appropriate film thickness has to be chosen to obtain reliable diffusion coefficients.

In case of MMMs, it is assumed that the film is a homogeneous layer in which all gas adsorbs equally. Although this assumption is by definition not valid for MMMs, it enables the observation of trends in the diffusion coefficient and this will yield insights in the transport behavior of MMMs. Alternatively it is possible to make a model which more accurately resembles the MMMs by separating the mass-uptake in a linear contribution of a fractional ethylene uptake by both the polymer and the Cu_3BTC_2 . However, by doing so, it proved to be impossible to gain accurate diffusion coefficients in Cu_3BTC_2 particles for a number of reasons. First, the size distribution of the particles proved to be quite broad which would allow discussion for the validity of Eq. (5). A similar argument can be made regarding the instantaneous pressure increase, which does not occur inside the membrane where the Cu_3BTC_2 particles reside. Additionally, the mass uptake in and on the particles might be limited by the presence of polymer material around the Cu_3BTC_2 MOF. Lastly, a distinct contribution of the mass uptake of the Cu_3BTC_2 particles in the 10 wt% MMM was too low, causing correlation between the fitting parameters, like the ethylene diffusion coefficients in the polymer and in the particles.

2.4. Gas permeation

Gas permeation through a dense membrane takes place according to the well-known solution–diffusion mechanism [24]:

$$P_i = S_i \times D_i \quad (8)$$

where the permeability coefficient P_i in Barrer (1 Barrer = $10^{-10} \text{cm}^3(\text{STP})\text{cm}/(\text{cm}^2 \text{s cmHg}) = 3.34 \times 10^{-16} \text{mol m}/(\text{m}^2 \text{s Pa})$) is the product of the solubility coefficient (S_i) ($\text{cm}^3(\text{STP})/(\text{cm}^3 \text{cmHg})$) and

the diffusion coefficient (D_i) (cm^2/s) of component i . The selectivity of a gas pair is the ratio of their permeability coefficients:

$$\alpha_{ij} = \frac{P_i}{P_j} = \left(\frac{D_i}{D_j} \right) \times \left(\frac{S_i}{S_j} \right) \quad (9)$$

where D_i/D_j is the diffusion selectivity and S_i/S_j the solubility selectivity of components i and j , respectively. Diffusion coefficients increase with decreasing penetrant size, increasing polymeric fractional free volume, increasing polymer chain flexibility, increasing temperature and decreasing polymer–penetrant interactions [25]. On the other hand, solubility coefficients increase with increasing polymer–penetrant interactions, decreasing temperature and increasing condensability of the penetrant.

3. Experimental

3.1. Materials

The matrix polymer Lenzing P84 polyimide (325 mesh, STD) was supplied by HP Polymer GmbH, Austria. *N*-methyl-2-pyrrolidone (NMP, 99% extra pure) was supplied by Acros Organics, Belgium, whereas the MOF copper benzene-1,3,5-tricarboxylate (Cu_3BTC_2) was obtained from Sigma-Aldrich (Basolite C300). A binary gas mixture of ethylene/ethane ($80/20 \pm 0.4 \text{ v/v}\%$) was used for gas permeation experiments and supplied by Praxair, the Netherlands. All chemicals were used as received.

3.2. Membrane preparation

3.2.1. Native P84 membranes

Before use, P84 polyimide powder was dried in a Heraeus Instruments Vacutherm vacuum oven at 100°C overnight. 15% (w/w%) P84 was dissolved in NMP and stirred at room temperature overnight, after which it was filtered through a $15 \mu\text{m}$ metal filter and degassed using an ultrasound bath for at least 30 min. The filtered and degassed solution was cast on a glass plate using a 0.47 mm casting knife. The remaining film was dried at room temperature under nitrogen for at least three days. Subsequently, the membrane was dried in a WTC Binder oven at 150°C and nitrogen flow for 24 h. Finally, the dried membrane was peeled off from the glass plate and dried in an oven at 60°C under nitrogen flow for at least three days.

3.2.2. Mixed matrix membranes

For MMM preparation, first a suspension of the MOF in NMP was prepared by mixing a certain amount of Cu_3BTC_2 in NMP. This suspension was stirred for 1 h and subsequently sonicated using a Branson 5210 ultrasound bath (40 kHz) for 15 min. After that, 10% of the total amount of dry P84 powder to be added, was mixed with the MOF/NMP suspension and stirred until completely dissolved. The remaining 90% of P84 powder was added subsequently and the mixture was stirred at least overnight. The suspension was degassed using an ultrasound bath for at least 30 min. The remaining suspension was used for membrane casting. Membranes were cast on a glass plate using a 0.47 mm casting knife. The cast membrane was dried at room temperature under nitrogen flow for at least two days, and subsequently in a WTC Binder oven at 150°C under nitrogen flow as well for 24 h to remove residual solvent. The dried membrane was peeled off from the glass plate and further dried in an oven at 60°C under nitrogen flow for at least three days. MMMs with 10, 20 and 40 wt% Cu_3BTC_2 were prepared and used for the experiments.

All prepared membrane samples were cut into circles with a diameter of 47 mm. The thickness of the final membranes, as

determined using an IP65 Coolant Proof digital Micrometer from Mitutoyo, ranged between 45 and $69 \mu\text{m}$.

3.3. SEM

Scanning electron microscopy (SEM) was used to investigate the homogeneity of the MOF distribution throughout the MMMs and compatibility between the MOFs and the polymer phase. After freezing and subsequent breaking of the membranes, the samples were dried in a vacuum oven at 30°C overnight and coated with a thin gold layer using a Balzers Union SCD040 sputtering device under argon flow. SEM images of the cross-sectional membrane area using a JEOL JSM-5600LV Scanning Electron microscope were taken. Data were processed using Semaphore software.

3.4. TGA

The thermal stability of the native P84 membrane, the Cu_3BTC_2 MOF and the $\text{Cu}_3\text{BTC}_2/\text{P84}$ MMMs with various loadings was performed using thermogravimetric analysis (TGA) on a Perkin Elmer TGA 4000. At least 5 mg of each sample was placed into a small aluminum sample holder. First the sample was held at 30°C for 1 min. Finally, the sample was heated to 900°C at a heating rate of 20°C per minute under a constant nitrogen flow of 20 mL per minute.

3.5. DSC

To determine the glass transition temperature (T_g) of native P84 and the Cu_3BTC_2 MMMs, differential scanning calorimetry (DSC) was performed on a Perkin Elmer DSC 8000. At least 2 mg of each sample was collected in an aluminum sample holder. The sample was held at 30°C for 1 min after which it was heated to the desired temperature. P84 polymer membrane samples were heated to 400°C , while the MMMs were heated till 350°C only at a constant heating rate of 100°C per minute. After reaching the end temperature, the sample was held for 1 min at this temperature and then cooled down to 30°C , again at a cooling rate of 100°C per minute. This cycle was repeated three times, and only the data from the last heating scan were used to determine the (T_g), which is defined as the midpoint of the heat capacity transition.

3.6. Gas sorption

Static and dynamic sorption measurements were performed on a magnetic suspension balance (MSB) (Rubotherm). Static sorption measurements allow determination of the sorption isotherms and the capacity and affinity constants for Cu_3BTC_2 MOFs according to Eq. (1) and native P84 and MMMs according to Eq. (3). Dynamic sorption measurements can be used to determine the diffusion constant of gas inside the Cu_3BTC_2 MOFs using to Eq. (5) and native P84 and the MMMs by means of Eq. (7). The mass uptake of the sample (m_t) was calculated according to Eq. (10):

$$m_t = w_t - (w_0 - V_t \times \rho_{\text{gas}}) \quad (10)$$

where w_0 is the weight of the sample (g) at zero sorption, V_t is the volume (cm^3) of the sample at time t (s) and ρ_{gas} is the density of the gas (g/cm^3). Archimedes principle was used to correct the recorded weight (w_t (g)) for buoyancy effects.

3.6.1. Static sorption experiments

The pure ethylene and ethane concentration of gas in the sample was calculated from the volume of the sample (calculated from the density of the sample as determined using a Micromeritics AccuPyc 1330 pycnometer at 26.0 ± 0.8 °C), the mass uptake of gas of the sample, and the molar volume and molecular weight of the gas. The molar volume of the gas was calculated using the Peng–Robinson equation of state.

A minimum of 50 mg of sample was used. Before each sorption run, the sample was degassed at 35 °C. A sorption run consisted of a stepwise increase in pressure until equilibrium was reached. When equilibrium was not reached within 24 h, a pseudo-equilibrium was taken at 24 h. All measurements were performed at a constant temperature of 35 ± 0.5 °C.

Mixed gas solubility selectivities in native P84 and MMMs were calculated using single gas parameters and Eq. (2), while taking into account the appropriate partial pressures during gas permeation measurements (ethylene/ethane 80/20 v%).

3.6.2. Dynamic sorption experiments

To determine the diffusion coefficient of ethylene in P84, Cu_3BTC_2 MOFs and Cu_3BTC_2 MMMs, dynamic sorption experiments were performed. Before the start of each experiment, the thickness of the membrane samples was measured and turned out to be 47, 48, 58 and 69 μm for P84 with 0, 10, 20 and 40 wt%, respectively. Prior to pressurization at 4 bar, the sample was evacuated for 10 h. Subsequently, the ratio of m_t/m_∞ was obtained as a function of time (s). Since in the case of membranes, complete equilibrium could not be established within the time scale of the experiment, in that case, the pseudo infinite mass uptake after 14 h was used. The obtained data were fitted using Eq. (7) to obtain the diffusion coefficients for the membrane samples while Eq. (5) was used to obtain the diffusion coefficient of ethylene in Cu_3BTC_2 MOFs.

3.7. Gas permeation

Gas permeation experiments using the constant volume, variable pressure method with vacuum at the permeate side as described elsewhere [26] were performed to evaluate the ethylene/ethane separating ability of native P84 membranes and all Cu_3BTC_2 MMMs. Partial pressures higher than 1 bar were replaced by their corresponding fugacities to correct for non-ideal behavior.

Alternating nitrogen and ethylene/ethane gas permeation measurements were performed on the same membrane samples. The nitrogen feed pressure was kept constant at 5 bar to investigate plasticization effects. The ethylene/ethane feed pressure was increased from 5 to 10 bar and eventually to 15 bar.

For mixed gas experiments, both feed and permeate were analyzed using a Varian 3900GC gas chromatograph equipped with an Alltech Alumina F-1 60/80 packed bed column at 150 °C. Enough permeate was collected to achieve a signal/noise (S/N) ratio of at least 10. Mixed gas selectivity was calculated according to Eq. (11):

$$\alpha_{ij} = \frac{y_i / y_j}{x_i / x_j} \quad (11)$$

where y_j and x_j are the downstream and upstream mole fractions of compound j , respectively.

4. Results and discussion

4.1. Membrane characterization

4.1.1. SEM

The morphologies of the cross-sectional membrane areas are investigated using SEM and shown in Fig. 1. A membrane made of pure P84 shows nothing except a dense polymer layer of approximately 53 μm , as can be seen in Fig. 1a. Fig. 1b shows that when 10% Cu_3BTC_2 is added to the polymer matrix, a layer of Cu_3BTC_2 and P84 forms at the bottom of the membrane. White circles indicate the

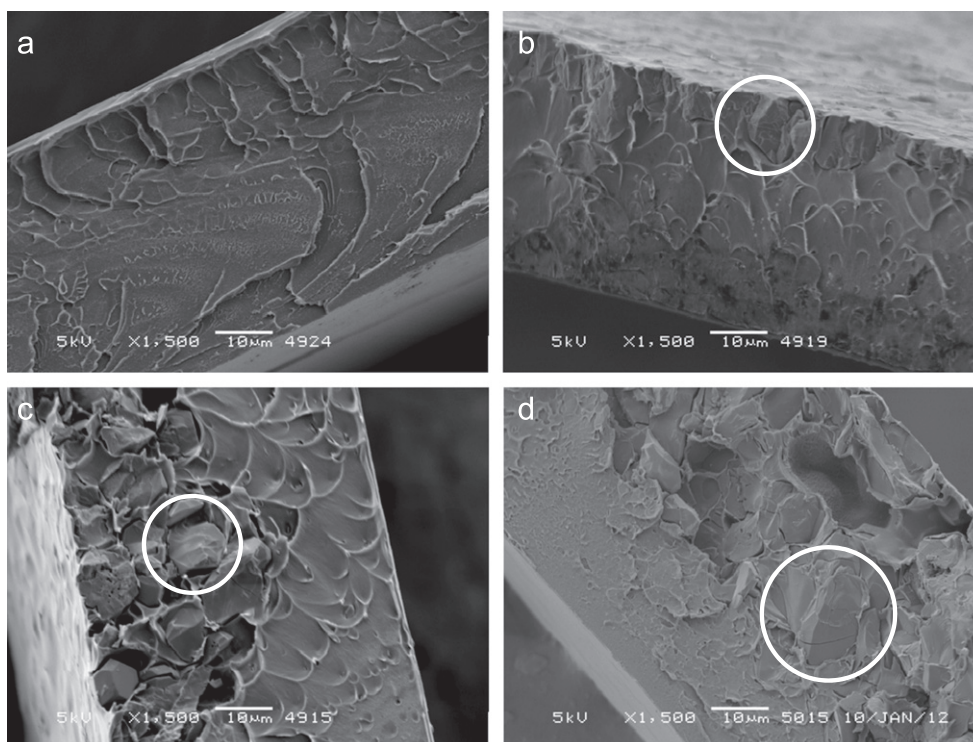


Fig. 1. SEM images of P84 MMMs with (a) 0 wt% Cu_3BTC_2 , (b) 10 wt% Cu_3BTC_2 , (c) 20 wt% Cu_3BTC_2 and (d) 40 wt% Cu_3BTC_2 . Particles are indicated by a white circle.

location of particles. The MOF crystals deposit at the bottom of the membrane during the membrane fabrication process when the solvent evaporates, creating an inhomogeneous membrane. Fig. 1c and d, with 20% and 40% Cu_3BTC_2 , respectively, show an increasingly thicker MOF-P84 layer with a decreasingly thinner pure P84 layer.

4.1.2. TGA

The effect of temperature on the degradation of native P84, MMMs at various loadings of Cu_3BTC_2 and pure Cu_3BTC_2 MOFs is shown in Fig. 2. The native P84 membrane (0% Cu_3BTC_2) has a weight loss of only 1.2% up to 175 °C. This is caused by evaporation of adsorbed solvent. An additional 9.5% of the weight is lost when the temperature is increased to 400 °C, which marks the start of the degradation process. P84 has lost 46% of its original weight at the final temperature of 900 °C.

Pure Cu_3BTC_2 MOFs show a weight loss of up to 26% when the temperature is increased to 200 °C. This indicated a loss of hydrated water [13]. At 350 °C, Cu_3BTC_2 loses 27% of its initial weight, which marks the start of the degradation process that last till the final temperature of 900 °C where only 32% of its initial weight is left.

The MMMs with 10, 20 and 40 wt% Cu_3BTC_2 show similar decomposition stages compared to the P84 membrane. When the temperature is increased up to 175 °C, they suffer from a weight loss of 1.3%, 3.2% and 5.7% due to the evaporation of hydrated water, respectively. This increasingly higher weight loss is related to the increased loading of hydrated Cu_3BTC_2 MOFs in the MMMs. Due to Cu_3BTC_2 's hygroscopic property as shown in [13,15], MMMs containing higher loadings of Cu_3BTC_2 have higher concentrations of water adsorbed. When the temperature is increased up to 400 °C, an additional 12%, 18% and 27% of the starting weight is lost, respectively. It is also visible that an extra decomposition stage appears between 350 and 380 °C when compared to P84. This extra stage is caused by the decomposition of Cu_3BTC_2 particles since it coincides with the Cu_3BTC_2 decomposition temperature. Therefore higher Cu_3BTC_2 loadings in the MMM cause higher weight losses. The degradation of the MMM continues, as the temperature is increased to 900 °C, and a final weight loss of 50%, 54%, 68% is recorded. This is a larger weight loss than the native P84 membrane because of the additional Cu_3BTC_2 added.

4.1.3. DSC

DSC analysis was performed on small pieces of P84 with 0, 10, 20 and 40 wt% Cu_3BTC_2 to determine the glass transition temperature and to investigate changes in chain flexibility when MOFs are added to the polymer matrix. As shown in Table 1, the T_g of P84 is visible at 345 °C.

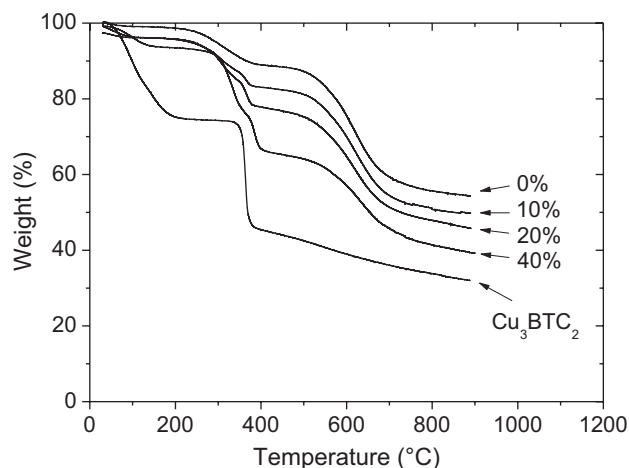


Fig. 2. TGA of Cu_3BTC_2 and P84 with various loadings of Cu_3BTC_2 .

Table 1

T_g of P84 MMMs with various Cu_3BTC_2 loadings.

Polymer	MOF type added	MOF loading (wt%)	T_g (°C)
P84	–	0	345
P84	Cu_3BTC_2	10	330
P84	Cu_3BTC_2	20	329
P84	Cu_3BTC_2	40	338

When 10 wt% Cu_3BTC_2 is added to the polymer matrix, a decrease in T_g of 15 °C to 330 °C is visible. This decrease in T_g is caused by disruption of physical crosslinks between the polymer chains due to the introduction of Cu_3BTC_2 crystals, which results in the formation of a more flexible intermediate phase between the polymer and the MOF. When the Cu_3BTC_2 loading is increased to 20 wt%, the T_g remains constant within the experimental error of the experiment. This suggests that the compatibility between the polymer and the MOF phase is still satisfactory. However, when the MOF loading is increased to 40%, the T_g increases again to 338 °C, which implies that there is less disruption of the physical crosslinks between the polymer chains. The deposition of high loadings of Cu_3BTC_2 limits interaction between P84 and all of the MOF crystals. These results in the possibility for P84 to form more physical crosslinks with itself compared to a loading of 20 wt% as was the case in native P84. This is expressed by a T_g between the native P84 and the 20 wt% MMM and even suggests the introduction of non-selective voids, as the interaction between the two phases is reduced.

Since the T_g of P84 is equal to the decomposition temperature of Cu_3BTC_2 as shown in Fig. 2, it is not possible to anneal the membranes and erase their history. In order to obtain comparable results, all membranes were fabricated such that all samples had the same history. Differences in sample history can affect permeabilities and selectivities as the result of physical aging [27].

4.1.4. Static gas sorption

Static gas sorption measurements were performed to characterize the sorption behavior of native P84 membranes and this is shown in Fig. 3. A dual mode sorption isotherm can be observed for both ethylene and ethane and the desorption data coincide with the sorption isotherm. This lack of hysteresis suggests that both ethylene and ethane do not induce plasticization in P84. When both sorption isotherms of ethylene and ethane are fitted with the dual-mode sorption model (Eq. (1)), the Henry's constants, the Langmuir capacity constants and the Langmuir affinity constants can be obtained and these are shown in Table 2. The low Henry constants for both ethylene and ethane indicate that the major sorption mechanism inside P84 is Langmuir sorption which takes place in the non-equilibrium excess volume occurring in glassy polymers [16]. Addition of MOF particles to the polymer matrix could affect and possibly disturb or alter this excess volume. This will be investigated hereafter with static gas sorption measurements in MMMs. The ideal ethylene/ethane sorption selectivity of P84 is almost constant at 1.5 over the whole fugacity range. This indicates that any form of selectivity present in native P84 membranes is mainly governed by diffusion selectivity. Therefore, enhancement of the solubility selectivity by addition of MOFs in MMMs could greatly enhance the selectivity.

The effect of Cu_3BTC_2 on the ethylene and ethane solubility in MMMs with 10 and 20 wt% Cu_3BTC_2 are shown in Fig. 4 as well as the ethylene and ethane solubility in native P84 and pure Cu_3BTC_2 MOFs.

Since the MMMs contain both polymer and MOF particles, the total amount of sorption is a combination of dual-mode and Sips sorption. Fitting the data with a linear combination of Eqs. (1) and

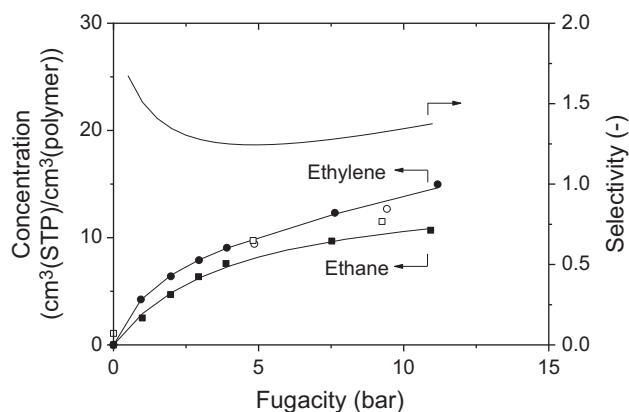


Fig. 3. Sorption isotherms (closed symbols) of ethylene (circle) and ethane (square) in native P84, corresponding desorption data (open symbols) and the ideal ethylene/ethane selectivity of native P84 as function of feed fugacities. Isotherms are fitted using the dual-mode sorption model (Eq. (1)).

Table 2

Fitted dual mode sorption and SIPS parameters in P84 with various wt% Cu_3BTC_2 of ethylene and ethane sorption isotherms.

Feed gas	wt% Cu_3BTC_2	Dual mode sorption model			SIPS model		
		C_H	b_i	k_D	C_S	b_S	n
Ethylene	0	8.82	0.73	0.64	–	–	–
	10	18.8	1.10	0.60	45.5	0.11	1.85
	20	29.2	1.59	0.84	68.6	0.12	2.17
	100	–	–	–	513	1.07	2.25
Ethane	0	14.9	0.24	0.00	–	–	–
	10	23.9	0.47	0.11	26.6	0.39	1.07
	20	31.4	0.92	0.20	35.5	0.72	1.13
	100	–	–	–	337	1.16	0.85

(3) was not possible; there are too many variables in that case to get non-correlated solutions. Therefore, to compare the obtained results with the sorption in pure Cu_3BTC_2 and native P84, the sorption isotherms of ethane and ethylene in the MMMs were fitted using both the dual mode sorption (Eq. (1)) and the Sips model (Eq. (3)) separately, where it was assumed that the MMMs consisted of one homogeneous phase. The obtained parameters for the dual mode sorption model and the Sips model are shown in Table 2.

When the dual mode sorption parameters for different wt% of Cu_3BTC_2 are compared in Table 2, an increase with increasing Cu_3BTC_2 loading is visible for all parameters for both ethylene and ethane. This implies that the addition of Cu_3BTC_2 increases the maximum sorption capacity and the affinity towards ethylene and ethane, but does not provide any additional sorption selectivity, since the ideal sorption selectivity does not increase.

Similar to the comparison of the dual mode sorption parameters, the Sips parameters of the MMMs in Table 2 can be compared to the Sips parameters of Cu_3BTC_2 MOF. The maximum sorption capacity, C_S , in 20 wt% P84 MMM is decreased by a factor 9 and 10 for ethylene and ethane, respectively, compared to the sorption in pure Cu_3BTC_2 MOFs. This reduction suggests that approximately 10% of the MMM sorption capacity is caused by the addition of MOFs, even though 20 wt% was added. This difference can be explained by sorption limitations in the Cu_3BTC_2 particles due to the surrounding polymer. DSC experiments shown in Table 1 showed that there is interaction between the polymer phase and the Cu_3BTC_2 particles up to 20 wt%. This might reduce the sorption capacity on the outside of the MOF where interaction with the polymer takes place, or limits the diffusion into Cu_3BTC_2 . The Sips affinity parameter of ethylene and ethane

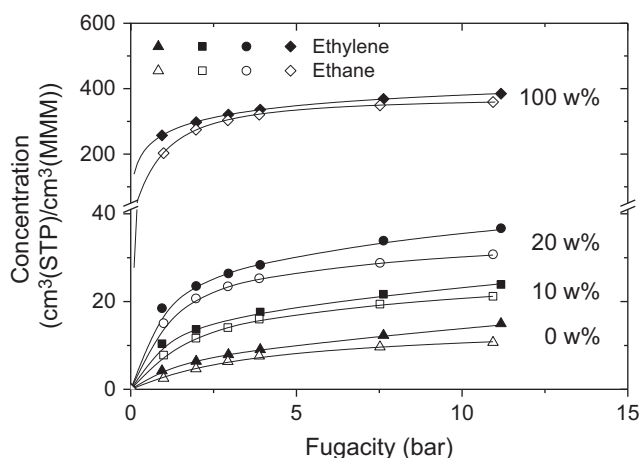


Fig. 4. Sorption isotherms of ethylene (closed) and ethane (open) in P84 with 0, 10, 20 wt% Cu_3BTC_2 and pure Cu_3BTC_2 particles (100%) as function of their corresponding fugacities. Isotherms displayed were fitted using Eq. (1) for native P84 and MMMs and Eq. (3) for pure Cu_3BTC_2 MOFs.

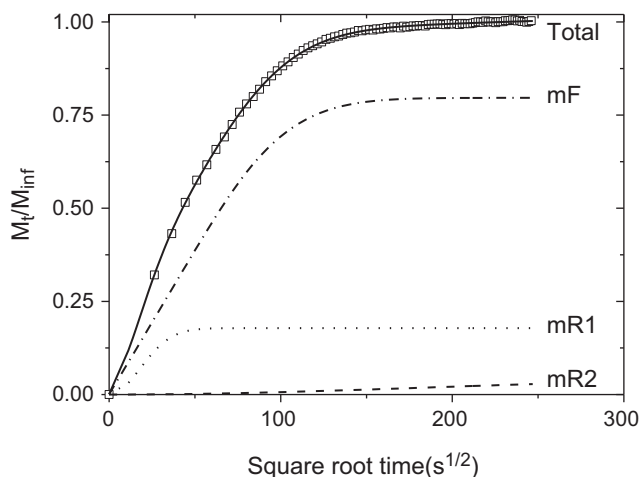


Fig. 5. Relative ethylene mass uptake (squares) as function of time. Solid black line is the best fit using Eq. (7), which is broken down into individual contributions of the Fickian, mF, (dash-dot line) first relaxational, mR1, (dot line) and second relaxational, mR2, (dash line) contribution.

for the MMM is lower than that for pure Cu_3BTC_2 , because 80 wt% of the MMM consists of P84 which has low affinity towards ethylene and ethane as is also shown in Table 2 for the dual-mode sorption model of native P84. Finally, the sorption intensity for ethylene decreases from 2.25 to 1.82 since the majority of the membrane consists of P84, which is assumed to adsorb only one molecule per sorption site according to the Langmuir model.

Addition of Cu_3BTC_2 particles to the P84 membranes appears to increase the maximum sorption capacity by a factor 2–3, while the ideal ethylene/ethane sorption selectivity is not significantly increased. Also, addition of Cu_3BTC_2 particles might have an influence on the diffusion coefficient, which will be discussed in the next paragraph.

4.1.5. Dynamic sorption

Dynamic sorption experiments were performed to determine the kinetic diffusion coefficients of the MMMs with various wt% Cu_3BTC_2 . It is important to verify whether all fitting parameters can be accurately obtained with the given film thickness. Therefore, data of a typical dynamic sorption experiment are shown in Fig. 5 and subdivided into its Fickian and relaxational contributions.

Fig. 5 shows that both relaxational contributions $mR1$ and $mR2$, can be separated from the Fickian mass uptake, which is necessary to accurately determine the diffusion coefficient. In case individual contributions would overlap, the fitted diffusion coefficient would be dependent on other fit parameters and not reflect the actual value. Although usually the relaxational contribution is a consequence of the Fickian absorption, it can be seen that in this case, the Fickian mass uptake continues while the first relaxational contribution is completed. However, this phenomenon is attributed to nano-scale defects or casting induced relaxed stresses in the polymer film, which allow for additional mass uptake once the Fickian diffusion process has started. Although this is technically not a relaxation process and would require additional experiments to fully understand, it is not relevant for the determination of trends of the Fickian diffusion coefficient.

Fig. 6 shows the ethylene concentration in P84 MMMs with various wt% of Cu_3BTC_2 . As expected from the static sorption experiments, higher loadings of Cu_3BTC_2 in P84 allow higher concentrations of ethylene to adsorb into the MMMs. It can also be seen that the ethylene concentrations at pseudo equilibrium are lower than reported in Fig. 4, which is due to variations in sample history caused by different measurement protocols for static and dynamic sorption measurements.

When the ethylene sorption in the MMMs is expressed in m_t/m_∞ as a function of time, diffusion coefficients can be fitted using Eq. (7). Based on these parameters, a theoretical permeability coefficient can be calculated according to Eq. (8) and it can be estimated what the theoretical effect of the added particles on the ethylene permeability is supposed to be. The solubility and diffusion coefficients of ethylene obtained from these dynamic sorption experiments are shown in Table 3, as well as the theoretical permeability in Barrer (P_B) and SI units (P_{SI}).

Table 3 shows that the increase in solubility is accompanied by an exponential increase in diffusion coefficient. As a result, the theoretical permeability coefficient of the Cu_3BTC_2 MMMs is expected to

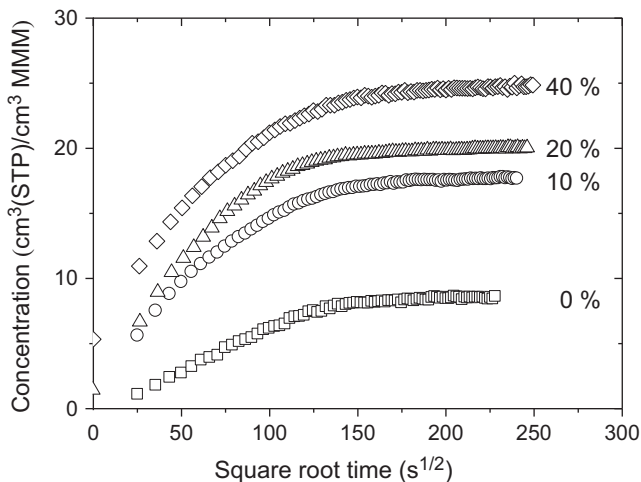


Fig. 6. Concentration of ethylene in native P84 and P84 with 10, 20 and 40 wt% Cu_3BTC_2 as function of time.

Table 3

Solubility coefficients, diffusion coefficients and theoretical permeability coefficients of ethylene in MMMs with various loadings of Cu_3BTC_2 .

	S (10^{-2} cm ³ /(cm ³ cmHg))	D (10^{-10} cm ² /s)	P_B (Barrer)	P_{SI} (10^{-18} mol m/(m ² s Pa)).
P84+0 wt% Cu_3BTC_2	2.8	2.8	0.08	27
P84+10 wt% Cu_3BTC_2	5.7	3.2	0.18	60
P84+20 wt% Cu_3BTC_2	6.6	6.1	0.40	134
P84+40 wt% Cu_3BTC_2	8.2	272	22.30	7458

show an even stronger exponential increase. When the results are investigated more closely, it can be deduced that the increase in theoretical permeability coefficient due to the addition of 10 wt% Cu_3BTC_2 is mainly caused by the increase in solubility. When higher Cu_3BTC_2 loadings are added to the polymer matrix, the increase in diffusion coefficient becomes the primary contribution to the increasing theoretical permeability coefficient. These findings imply that in theory MMM permeabilities should increase with increasing Cu_3BTC_2 loading as a result of either removed diffusion limitations in the polymer or by introduction of non-selective voids. Experimental determination of the gas permeation behavior could resolve this question as the removal of diffusion limitations will show enhanced selectivities, opposite to the introduction of non-selective voids which will reduce selectivities to values close to the native membrane material. This will be further discussed in the next paragraph.

4.1.6. Gas permeation measurements

4.1.6.1. Effect of Cu_3BTC_2 loading. Fig. 7 shows the ethylene permeability and ethylene/ethane selectivity at various loadings of Cu_3BTC_2 added to P84. Fig. 7a shows that the ethylene permeability of 17×10^{-18} mol m/(m² s Pa) does not increase with increasing Cu_3BTC_2 loading up to 20 wt%. Especially when the standard deviation between the samples is considered, the small permeability increase at 20% Cu_3BTC_2 can be considered insignificant. The measured ethylene permeability of native P84 is very close compared to the calculated ethylene permeability of 27×10^{-18} mol m/(m² s Pa), which was based on the solubility and diffusion coefficients shown in Table 3. Discrepancies between these two permeability values are most likely the result of differences in measurement techniques. Mainly the fact that for the theoretical permeability, the solubility parameter was determined using feed gas on all sides of the membrane, while the experimental permeability was determined using vacuum at the permeate side, could contribute to this. An increasingly larger discrepancy occurs when the Cu_3BTC_2 loading is further increased due to the different operating conditions.

The effect of Cu_3BTC_2 loading on the ethylene/ethane selectivity is shown in Fig. 7b. There is a clear correlation visible between the selectivity and the amount of Cu_3BTC_2 ; when the Cu_3BTC_2 loading is increased from 0% to 20%, the ethylene/ethane selectivity increases from 4.1 to 7.1, respectively. These findings are consistent with a combination of Case 0 (ideal polymer-particle interaction) and Case I (rigidified polymer layer around particle) or Case IV (clogged porous particles), which would result in a constant permeability and an increasing selectivity as the particle loading increases. However, the absence of an increase in T_g and a calculated reduction in diffusion coefficient eliminates the possibility of a Case I situation and makes a combination of Case 0 and Case IV more probable. When the Cu_3BTC_2 loading is even further increased to 40 wt%, the ethylene/ethane selectivity drops to 5.0, which is a significant reduction. At the same time, the ethylene permeability increases dramatically to 25.5×10^{-18} mol m/(m² s Pa). These results indicate that due to the large amount of Cu_3BTC_2 added to the polymer matrix, in combination with their inhomogeneous distribution, non-selective voids are created when 40% MOF is added to the polymer (Case II).

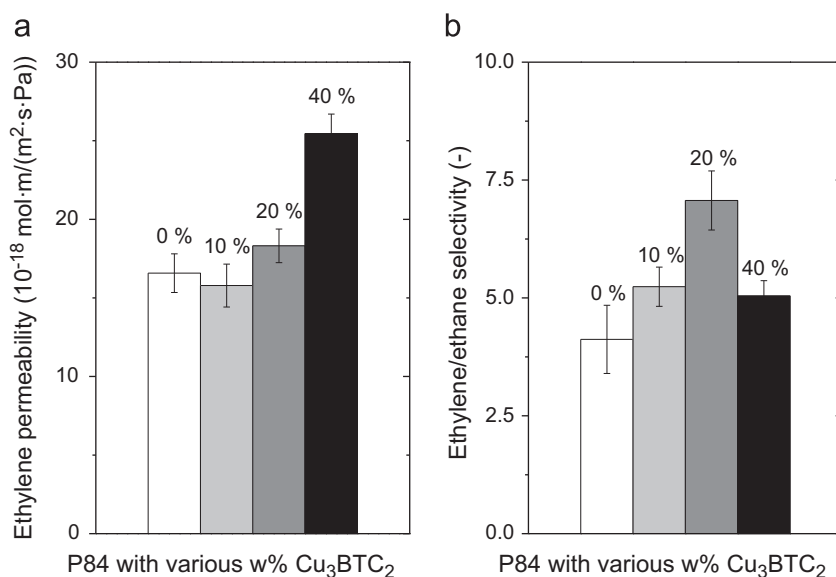


Fig. 7. (a) Ethylene permeability and (b) ethylene/ethane selectivity ($\pm 2\sigma$) of P84 with various amounts of Cu₃BTC₂ MMMs at 5 bar mix gas feed pressure.

The lack of increase in permeability up to 20 wt% is surprising because numerous reports mention a simultaneous increase in both selectivity and permeability or permeance of the fast moving component when MOFs are added to the polymer matrix [5–7, 11,28,29]. Although many researchers investigate different, sometimes self-synthesized MOFs, the increase in permeability or permeance has also been observed for the commercially available MOFs used in this study [5,28]. Basu et al. observed a minor increase in carbon dioxide/nitrogen selectivity with a strongly increasing carbon dioxide permeance, as well as an increasing carbon dioxide/methane selectivity accompanied by an increasing carbon dioxide permeance [5]. Although the authors used Matrimid as polymer matrix as opposed to P84, no significant changes would be expected since both materials are polyimides. In addition, the inherent low permeability of P84 towards ethylene is expected to give an even larger enhanced permeability when Cu₃BTC₂ is added as dispersed phase. The constant ethylene permeability with varying amounts of Cu₃BTC₂ demonstrates the absence of non-selective voids between the MOF particles and the polymer matrix. If non-selective voids were present, a clear correlation between the ethylene permeability and the MOF loading in the MMM would have been observed. Because of this lack of defects, and the fact that the difference in polymer matrix used cannot explain the observed constant permeability, only differences in penetrant–MMM interaction can explain these findings. Although it was shown by dynamic sorption measurements that the ethylene diffusion coefficient in MMMs, shown in Table 3, increases with increasing Cu₃BTC₂ loading, this is not related to the rate of desorption and therefore only confirms that ethylene diffuses faster in and not per definition through the MMM. Ethylene could exhibit strong interactions with the MMM and be slowed or immobilized and consequently clog the porous Cu₃BTC₂ MOFs causing Case IV. Because of Cu₃BTC₂'s high sorption capacity for ethylene as shown in Fig. 4, it is very likely that interactions of ethylene with Cu₃BTC₂ take place, which in turn, might lower the diffusion coefficient during permeation experiments if these interactions are strong. Future work will need to be done to better understand the transport mechanism of gasses through MMMs.

Given the above, it is clear that facilitated ethylene transport does not take place through the Cu₃BTC₂ crystals. Since the sorption capacity of Cu₃BTC₂ is an order of magnitude higher than for P84, it is evident that the gas can enter all or part of the pores present in the crystals. Although larger amounts of gas can adsorb into MMMs, diffusion through the MMMs is not enhanced and even reduced with increasing Cu₃BTC₂ loading added to the polymer matrix, which results in a constant ethylene permeability. As shown with dynamic sorption measurements, the fact that ethylene diffuses faster in MMMs with higher Cu₃BTC₂ loadings, shows that this is unrelated to the diffusion behavior of penetrants through a MMM in gas permeation experiments.

4.1.6.2. Effect of feed pressure. Plasticization increases the permeability of the membranes while reducing the selectivity as a result of excessive polymer swelling. To investigate this effect in MMMs, feed pressures were varied and selectivities and permeabilities were measured for Cu₃BTC₂ MMMs. The results of the ethylene permeabilities and the ethylene/ethane selectivities are presented in Fig. 8a and b, respectively. Fig. 8a shows a slight decrease in ethylene permeability for native P84 with increasing feed pressure. This is consistent with the dual-mode behavior in glassy polymers and P84 shows no signs of induced plasticization [16,30]. A similar permeability reduction is observed when various wt% of Cu₃BTC₂ are added to the P84 matrix, showing that adding Cu₃BTC₂ does not induce plasticization effects up to 15 bar mixed gas feed pressure. Fig. 8b shows no significant decrease in selectivity of the native P84 with increasing feed pressure up to 15 bar. This indicates that no significant plasticization takes place in the pressure range investigated, which is in agreement with similar studies for other gasses [31,32]. Also, no reduction in selectivity is observed when various wt% of Cu₃BTC₂ are added to the polymer matrix. This, in combination with the absence of an increasing permeability with increasing feed pressure, indicates that plasticization phenomena do not occur within this study.

Since both the permeability (Fig. 8a) and solubility (Fig. 4) are now determined over a pressure range up to 15 bar mixed gas feed pressure, it is possible to calculate the diffusion coefficients of ethylene at various mixed gas feed pressures according to Eq. (8)

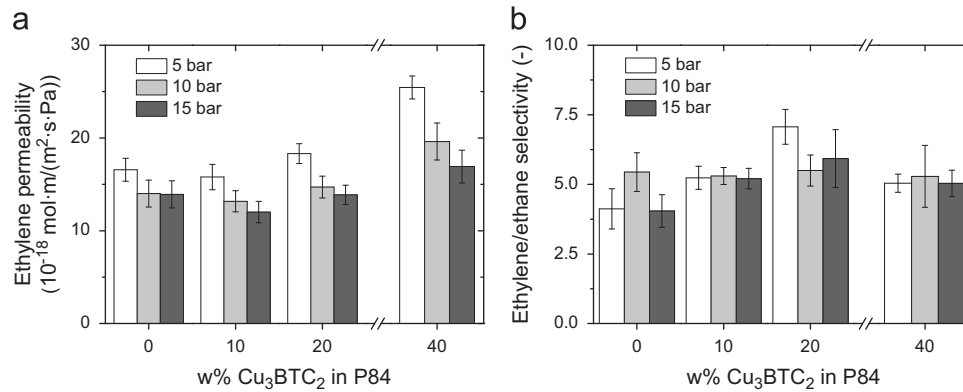


Fig. 8. Effect of mixed gas feed pressure on the (a) ethylene permeability and (b) ethylene/ethane selectivity ($\pm 2\sigma$) for P84 MMMs with various wt% of Cu_3BTC_2 .

Table 4

Measured permeability coefficients (10^{-18} mol m/(m^2 s Pa)), calculated solubility coefficient (10^{-3} mol/(m^3 Pa) based on Eqs. (2) and (4), and calculated diffusion coefficient (10^{-15} m^2/s) based on Eq. (8) for ethylene in P84 with various loadings of Cu_3BTC_2 at various mixed gas feed pressures.

	5 bar			10 bar			15 bar		
	P	S	D	P	S	D	P	S	D
P84+0% Cu_3BTC_2	16.6	1.0	16.8	14.0	0.7	20.3	13.9	0.6	24.2
P84+10% Cu_3BTC_2	15.8	1.9	8.5	13.2	1.2	11.4	12.0	0.9	13.4
P84+20% Cu_3BTC_2	18.3	2.9	6.3	14.7	1.8	8.4	13.9	1.3	10.4

Table 5

Calculated mixed gas permeability and diffusivity selectivities based on Eq. (9) and solubility selectivity based on Eqs. (2) and (4), for P84 MMMs with various loadings of Cu_3BTC_2 at various mixed gas feed pressures.

	5 bar			10 bar			15 bar		
	α_P	α_S	α_D	α_P	α_S	α_D	α_P	α_S	α_D
P84+0% Cu_3BTC_2	4.1	2.5	1.7	5.4	3.0	1.8	4.0	3.5	1.2
P84+10% Cu_3BTC_2	5.2	2.0	2.6	5.3	2.2	2.4	5.2	2.3	2.3
P84+20% Cu_3BTC_2	7.1	1.7	4.0	5.5	1.9	3.0	5.9	1.9	3.0

and compare these with the diffusion coefficients obtained by dynamic sorption experiments. These results are shown in Table 4. Since the solubility coefficient of ethylene at 5 bar mixed feed gas increases 190% to 2.9 when 20 wt% Cu_3BTC_2 is added, the constant permeability coefficient of ethylene consequently lowers the diffusion coefficient to 6.3 at 5 bar mixed feed pressure. Similarly, at 10 and 15 bar mixed gas feed pressure, the ethylene solubility increases with increasing Cu_3BTC_2 loading and therefore, the diffusion coefficient decreases with increasing Cu_3BTC_2 loading. As mentioned in the introduction, a decrease in diffusion coefficient with increasing particle loading has also been observed in literature by Adams et al. for carbon dioxide, oxygen, nitrogen and methane when 15 wt% Cu TPA MOF was added to a poly(vinyl acetate) matrix and attributed this to immobilization of penetrant inside the MMMs [12].

However, the solubility coefficient is decreasing with increasing feed pressure at constant Cu_3BTC_2 loading. As a result, the diffusion coefficient increases with increasing feed pressure. Similar to ethylene, the mixed gas permeability, solubility and diffusion coefficients of ethane can be determined for various Cu_3BTC_2 loadings at various pressures. This leads subsequently to the calculations of the mixed gas permeability, solubility and diffusion selectivity, shown in Table 5 for P84 with Cu_3BTC_2 loadings up to 20% at feed pressures from 5 to 15 bar. At constant pressure, the permeability selectivity

increases with increasing Cu_3BTC_2 loading. At 10 bar feed pressure, this effect is only slightly visible because of the relatively large standard deviations. Furthermore, the solubility selectivities decrease with increasing Cu_3BTC_2 loading which in return, lead to an increase in diffusion selectivity up to 120%. When the Cu_3BTC_2 loading remains constant, it can be observed that the permeability selectivity is slightly reduced with increasing feed pressure. However, the solubility selectivity increases with increasing feed pressure, which results in a reduction of the diffusion selectivity.

From these data, it is clear that the main mechanism responsible for the increase in selectivity with increasing Cu_3BTC_2 loading is due to an increase in diffusion selectivity caused by the Cu_3BTC_2 particles. Sorption experiments shown in Fig. 4 already revealed that the ideal sorption selectivity in Cu_3BTC_2 was low and therefore, no increase in selectivity based on enhanced solubility selectivity could be expected.

Sorption experiments shown in Fig. 4 showed an increase in ethylene concentration when Cu_3BTC_2 particles were added to the P84 matrix. It is hypothesized that this increased concentration of ethylene is immobilized inside the MMMs and hinders the diffusion of ethane through the MMM. This would ultimately result in constant permeabilities and increased selectivities with increased loadings of Cu_3BTC_2 added to the polymer matrix.

5. Conclusions

P84 MMMs with various amounts of Cu_3BTC_2 have been successfully prepared. Ethylene/ethane selectivity increased up to 73% from 4.1 to 7.1 with increasing Cu_3BTC_2 loading up to 20 wt%, while the permeability remained constant at 17×10^{-18} mol m/(m^2 s Pa), which confirms, in combination with DSC data, the absence of non-selective voids in the MMMs. The ethylene solubility coefficient increased from 1.0 to 2.9×10^{-3} mol/(m^3 Pa) with increasing loading of Cu_3BTC_2 , while the diffusion coefficient decreased from 16.8 to 6.3×10^{-15} m^2/s . This indicates that a large part of the ethylene is immobilized inside the MMM, hindering the diffusion of ethane and to some extent its own. This is reflected in the increase in diffusion selectivity and the reduction of solubility selectivity with increasing Cu_3BTC_2 loading. Increasing the loading beyond 20 wt% led to the formation of non-selective voids, which resulted in increased permeabilities up to 26×10^{-18} mol m/(m^2 s Pa) with selectivities being reduced to that of native P84. Increasing the feed pressure from 5 to 15 bar resulted in slight reductions of permeabilities, which is typical dual-mode behavior in glassy polymers. In addition, the increase in feed pressure showed an increase in solubility selectivity and therefore, a reduction in diffusion selectivity.

Acknowledgements

This project is financially supported by AgentschapNL. The authors would like to thank ECN, Dow and SolSep for the fruitful discussions.

References

- [1] 232nd ACS national meeting, San Francisco, Sept. 10–14, Chemical and Engineering News 84 (2006) 59–236.
- [2] L.M. Robeson, The upper bound revisited, *J. Membr. Sci.* 320 (2008) 390–400.
- [3] L.M. Robeson, W.F. Burgoyne, M. Langsam, A.C. Savoca, C.F. Tien, High performance polymers for membrane separation, *Polymer* 35 (1994) 4970–4978.
- [4] A. Motelica, O.S.L. Bruinsma, R. Kreiter, M. Den Exter, J.F. Vente, Membrane retrofit option for paraffin/olefin separation—a technoeconomic evaluation, *Ind. Eng. Chem. Res.* 51 (2012) 6977–6986.
- [5] S. Basu, A. Cano-Odena, I.F.J. Vankelecom, MOF-containing mixed-matrix membranes for CO₂/CH₄ and CO₂/N₂ binary gas mixture separations, *Sep. Purif. Technol.* 81 (2011) 31–40.
- [6] C. Zhang, Y. Dai, J.R. Johnson, O. Karvan, W.J. Koros, High performance ZIF-8/6FDA-DAM mixed matrix membrane for propylene/propane separations, *J. Membr. Sci.* 389 (2012) 34–42.
- [7] Y. Dai, J.R. Johnson, O. Karvan, D.S. Sholl, W.J. Koros, Ultem®/ZIF-8 mixed matrix hollow fiber membranes for CO₂/N₂ separations, *J. Membr. Sci.* 401–402 (2012) 76–82.
- [8] J. Hu, H. Cai, H. Ren, Y. Wei, Z. Xu, H. Liu, Y. Hu, Mixed-matrix membrane hollow fibers of Cu₃(BTC)₂ MOF and polyimide for gas separation and adsorption, *Ind. Eng. Chem. Res.* 49 (2010) 12605–12612.
- [9] O.G. Nik, X.Y. Chen, S. Kaliaguine, Functionalized metal organic framework-polyimide mixed matrix membranes for CO₂/CH₄ separation, *J. Membr. Sci.* 413–414 (2012) 48–61.
- [10] J.A. Thompson, K.W. Chapman, W.J. Koros, C.W. Jones, S. Nair, Sonication-induced Ostwald ripening of ZIF-8 nanoparticles and formation of ZIF-8/polymer composite membranes, *Microporous Mesoporous Mater.* 158 (2012) 292–299.
- [11] H.B. Tanh Jeazet, C. Staudt, C. Janiak, Metal-organic frameworks in mixed-matrix membranes for gas separation, *Dalton Trans.* 41 (2012).
- [12] R. Adams, C. Carson, J. Ward, R. Tannenbaum, W. Koros, Metal organic framework mixed matrix membranes for gas separations, *Microporous Mesoporous Mater.* 131 (2010) 13–20.
- [13] S.S.-Y. Chui, S.M.-F. Lo, J.P.H. Charmant, A.G. Orpen, I.D. Williams, A chemically functionalizable nanoporous material [Cu₃(TMA)₂(H₂O)₃]*n*, *Science* 283 (1999) 1148–1150.
- [14] K.K. Kopeć, S.M. Dutczak, M. Wessling, D.F. Stamatialis, Chemistry in a spinneret—on the interplay of crosslinking and phase inversion during spinning of novel hollow fiber membranes, *J. Membr. Sci.* 369 (2011) 308–318.
- [15] J. Ploegmakers, S. Japip, J. Nijmeijer, Mixed matrix membranes containing MOFs for ethylene/ethane separation. Part A: Membrane preparation and characterization, *J. Membr. Sci.*, <http://dx.doi.org/10.1016/j.memsci.2012.11.014>, in press.
- [16] D.R. Paul, Gas sorption and transport in glassy polymers, *Berichte der Bunsengesellschaft für physikalische Chemie* 83 (1979) 294–302.
- [17] R. Sips, On the structure of a catalyst surface, *J. Chem. Phys.* 16 (1948) 490–495.
- [18] D.D. Do, *Adsorption Analysis Equilibria and Kinetics*, Imperial College Press, London, 1998.
- [19] S. Al-Asheh, F. Banat, R. Al-Omari, Z. Duvnjak, Predictions of binary sorption isotherms for the sorption of heavy metals by pine bark using single isotherm data, *Chemosphere* 41 (2000) 659–665.
- [20] J. Crank, *The Mathematics of Diffusion*, 2nd ed., Clarendon Press, Oxford, 1979.
- [21] J. Crank, G.S. Park, *Diffusion in Polymers*, Academic Press, London and New York, 1968.
- [22] A.R. Berens, H.B. Hopfenberg, Diffusion and relaxation in glassy polymer powders: 2. Separation of diffusion and relaxation parameters, *Polymer* 19 (1978) 489–496.
- [23] T. Visser, M. Wessling, When do sorption-induced relaxations in glassy polymers set in? *Macromolecules* 40 (2007) 4992–5000.
- [24] J.G. Wijmans, R.W. Baker, The solution-diffusion model: a review, *J. Membr. Sci.* 107 (1995) 1–21.
- [25] Y. Yampolskii, I. Pinnau, B.D. Freeman, *Materials Science of Membranes*, John Wiley & Sons Ltd., Chichester, 2007.
- [26] J.N. Barsema, G.C. Kapantaidakis, N.F.A. Van Der Vegt, G.H. Koops, M. Wessling, Preparation and characterization of highly selective dense and hollow fiber asymmetric membranes based on BTDA-TDI/MDI co-polyimide, *J. Membr. Sci.* 216 (2003) 195–205.
- [27] J. Xia, T.-S. Chung, P. Li, N.R. Horn, D.R. Paul, Aging and carbon dioxide plasticization of thin polyetherimide films, *Polymer* 53 (2012) 2099–2108.
- [28] S. Basu, A. Cano-Odena, I.F.J. Vankelecom, Asymmetric Matrimid®/[Cu₃(BTC)₂] mixed-matrix membranes for gas separations, *J. Membr. Sci.* 362 (2010) 478–487.
- [29] T.H. Bae, J.S. Lee, W. Qiu, W.J. Koros, C.W. Jones, S. Nair, A high-performance gas-separation membrane containing submicrometer-sized metal-organic framework crystals, *Angew. Chem. Int. Ed.* 49 (2010) 9863–9866.
- [30] V. Stannett, The transport of gases in synthetic polymeric membranes: an historic perspective., *J. Membr. Sci.* 3 (1978) 97–115.
- [31] A. Bos, I. Pünt, H. Strathmann, M. Wessling, Suppression of gas separation membrane plasticization by homogeneous polymer blending, *AIChE J.* 47 (2001) 1088–1093.
- [32] T. Visser, N. Masetto, M. Wessling, Materials dependence of mixed gas plasticization behavior in asymmetric membranes, *J. Membr. Sci.* 306 (2007) 16–28.